Simulation of colloid thruster droplet evolution using kinetic Monte Carlo

IEPC-2019-A-530

Presented at the 36th International Electric Propulsion Conference
University of Vienna, Austria
September 15-20, 2019

Neil Mehta* and Deborah A. Levin†
University of Illinois, Urbana-Champaign, Illinois, 61801, USA

The disintegration of large ionic liquid (IL) droplets emitted during the electrospray process when traversing through the region between the capillary and the extractor plane is important in determining the final electrospray products. Due to the computational cost associated with molecular dynamics (MD), simulations of droplet fragmentation are limited on the length and time scales of several nanometers and nanoseconds. In this work, we propose a kinetic Monte Carlo (kMC) approach to study droplet fragmentation. The kMC algorithm relies on the ion emission model and Rayleigh instability equation to determine fragmentation rate of the IL droplet. Using kMC, we were able to replicate the fragmentation behavior of EMIM-BF_4 droplet, similar to that observed from MD simulation.

I. Introduction

Colloid thrusters are a class of nano-thrust electric propulsion devices which can be used on small satellites for orbit correction or station keeping. These devices use ILs as propellants, such that, the IL is pressure fed through a capillary into a region of applied electric field. ILs are defined as salts having a melting point less than room temperature (373 K) and, have the ability to form a Taylor cone and emit ions. The electric field conducts the IL, causing the emission of a fine jet of ions from a Taylor[1] cone formed at the mouth of the capillary. The emission from the Taylor cone is also known as an electrospray and it has numerous applications other than in electric propulsion. Electrosprays have been used extensively in the field of micro-fabrication allowing controlled deposition[2] of metals as well as microfilm deposition on surfaces,[3] microcircuit manufacturing,[4] and ion beam lithography.[5] Electrosprays have also been used in bio-medical engineering,[6,7] for the analysis of biological tissues.[8]

Depending on the mode of operation mode as well as the electrochemical properties, ILs can either emit individual ion species or sub-micron sized droplets (colloids) that are

*PhD Candidate, Department of Aerospace Engineering, and namehta4@illinois.edu
†Professor, Department of Aerospace Engineering, and deblevin@illinois.edu

accelerated by the electric fields, generating high exhaust velocities. A large number of ILs can be used as propellants for electrosprays,[9,10] to cater to the wide range of performance requirements. Therefore, it is necessary to have experimental and simulation based ability to predict the thrust, required voltages, and mode of operation to design electrospray devices. We have used MD, which is a particle based method that allows for atomistic scale understanding of electrosprays.[11] The availability of accurate inter-atomic potentials makes it possible to model various ILs typically used in electrospray thrusters.

Colloid thruster performance and operational characteristics, such as, emission species and currents, have been traditionally measured from experiments.[12] These experiments are beneficial in determining the total operational life of the electrospray thruster as well as its total power requirements. These experiments are conducted over a length and time scales of micro-meters and micro-seconds. However, due to the high computational cost associated with MD simulations, the tenable simulations currently possible are at length and time scales of nano-meters and nano-seconds.[13] While MD simulations can provide accurate correlation between potential energy of the IL and the Taylor cone formation, and the emission closest to the tip of the cone, the differences in the length and time scale are particularly noticeable in the motion of large droplets emitted from the Taylor cone. The smaller emission ion species will travel through the applied electric field without disintegrating due to stronger Coulomb interactions in smaller ion species. However, the larger ion aggregates will undergo further fragmentation into smaller species in the duration it traverses through the external electric field between the Taylor cone and the extractor. Therefore, it is necessary to formulate a scale-bridging technique which allows for modeling the motion of MD predicted near cone emissions through the simulated electric field over a length and time scales of micrometers and microseconds. This will enable direct comparison between the experiments and simulations.

Studies on understanding droplet fragmentation have used high speed photography,[14,15] rapid solidification using sol-gel,,[16] as well as, MD simulations.[17,18] MD simulations were performed by Ichiki, *et al.*,[17] for a system of water molecules charged by Cl^-.[17] Similarly, Marginean, *et al.*[18] used pronated diglycine molecules[18] to study the effect of Rayleigh critical limit and the evolution of nano jet from the droplets. While shape deformation[19] and mass loss can be analyzed using experimental[20] methods, theoretical models are preferred for providing insight into charge reduction during the droplet disintegration process. Widely accepted theoretical models for droplet fragmentation include the charged residue mechanism (CRM)[21] and the ion evaporation mechanism (IEM).[22] The CRM postulates that smaller ion species are emitted from the primary or original droplet due to recurring instabilities generated within the droplet structure, as predicted by the Rayleigh theory.[23] The IEM describes the disintegration process using first order reaction kinetics. We can use parts of the two theoretical models to create a numerical model capable of replicating the droplet fragmentation process over a time scale of microseconds. It would be ideal if the near field emission products from MD simulations are used as initial condition for scale-bridging to larger length and time-scales using kMC.

kMC is a probabilistic method based on the "process list" algorithm, which is capable of simulating the time evolution of processes. kMC simulations have been traditionally used to replicate Ising model[24] and surface topology evolution.[25,26] In this work, we have implemented kMC algorithm to model ILs droplet evolution due to external electric field. A core pre-requisite for any kMC simulation is the need to determine the process rate, which will relate fragmentation time with the simulated elapsed time. For this purpose, elements from

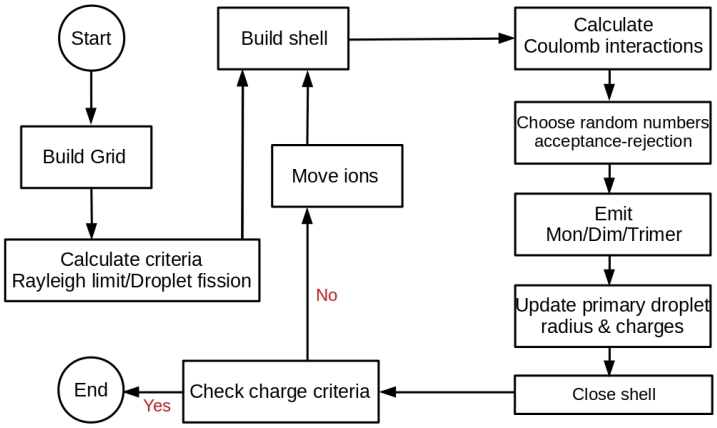

Figure 1. Modified kMC algorithm for droplet fragmentation.

the CRM and IEM model have been used to determine Rayleigh limit and time between successive emissions, as shall be discussed in detail in the next section. In this work, we have performed kMC droplet fragmentation simulations of 1-ethyl-3-methylimidazolium Tetrafluoroborate (EMIM-BF_4) and 1-ethyl-3-methylimidazolium etylsulfate (EMIM-$EtSO_4$).

II. Numerical methods used for kMC simulations

The modified kMC algorithm developed for performing droplet fragmentation is shown in Fig. 1. kMC relies on the N-fold way algorithm to model time-evolution of multiple independent events. This is well suited for modeling droplet fragmentation because, we have concurrent emission of a monomer, dimer, or trimer from the primary droplet which will be referred to in the kMC algorithm as events n_0, n_1, and n_2, respectively. Every iteration of the kMC simulation represents an event occurring and the time elapsed between two events, *i.e.* ion emission is added to the total elapsed simulation time. This makes it possible to have a time accurate representation of droplet fragmentation. kMC simulations are performed using a uniform grid, such that flags are assigned to each cell in the grid to represent either an empty space or a volume occupied by either a cation or an anion. The grid for the droplet fragmentation simulations, which includes the empty region surrounding the primary droplet, is constructed using 60 x 60 x 60 grid cells representing a simulated domain of size 0.3 x 0.3 x 0.3 µm. A droplet is generated in the center of the domain with a radius of 56 Å, which is a typical diameter for droplets observed to emit from our MD simulations.[27] For both, EMIM-BF_4 and EMIM-$ETSO_4$, the size of each cell in the kMC grid equals the size of the EMIM cations and, BF_4 and $EtSO_4$ anions, approximately 5.0 Å. The droplet is constructed by considering all cells within a radius of 60 Å from the center of the domain to be either a cation or an anion. Droplets can be defined as a combination of nine or more cation-anion pairs attached to either a number of excess cations or anions, depending on the electrospray mode of operation. If a negative potential is applied at the extractor ring, the electrospray

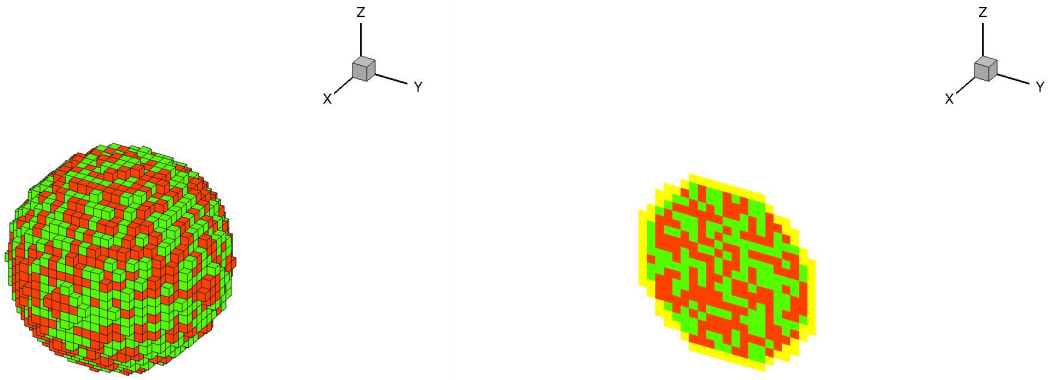

(a) kMC droplet geometry (b) Shell generated around kMC droplet geometry

Figure 2. Schematic of the kMC droplet grid and the shell of emission eligible kMC sites. Green and red sites represent cations and anions, respectively. Each site has a dimension of 5 x 5 x 5 Å.

will emit positive ion species and therefore, is defined as operating in the positive mode, and vice-versa. In this work, we have used the electric field values obtained in the domain for an applied potential of -17 V at the extractor plane which is at a distance of 1,000 Å from the mouth of the capillary. Droplets emitted during the electrospray process will have a biased total charge, meaning that for the positive emission mode, a droplet may have greater than 150 cations than the anions in the droplet. This is defined as a charge bias, b, of the droplet. An example of a kMC droplet with 150 cation bias is shown in Fig. 2(a), where cations and anions are represented by green and red cells, respectively. This bias was determined from a prototypical droplet emitted during the MD electrospray simulation.[27] The kMC droplet is comprised of 3019 cations and 2868 anions giving it a net positive charge of +150 e.

Droplet fragmentation will occur primarily due to Rayleigh instability within the droplet and the energy provided by the external electric field. Irrespective of the presence of electric field, droplets with charge greater than the Rayleigh limit will undergo Rayleigh instability, whereby, charges over the Rayleigh limit will fragment from the droplet. The Rayleigh limit for the droplet can be calculated as,[18]

$$z^2 = b^2 - \frac{64\pi^2\epsilon_0\gamma r^3}{e^2} \tag{1}$$

where, z is the number of charges, $\epsilon_0 = 8.8541 \times 10^{-12}$ F/m is the permittivity of vacuum, γ is the surface tension, $e = 1.60217 \times 10^{-19}$ C is the elementary charge, and r is the radius of the droplet. In contrast, in the presence of an external electric field, Hogan, Jr, *et al.*[28] using the aspects of the IEM and CRM theory estimated that the number of charges on an ion-emitting droplet can be calculated as,

$$z = \frac{\pi\epsilon_0 E^* r^2}{4e} \tag{2}$$

where, E^* is the amplitude of the applied external electric field. At the start of kMC droplet fragmentation simulation, the higher excess charge given by either Eqs. 1 or 2, is selected as the determining criterion for fragmentation.

The fragmentation process is initialized by flagging only the outermost shell of ions as eligible for emission from the primary droplet. From our previous MD simulations, it was observed that emission of ions occurs primarily from an outermost shell of the droplet and flagging shell ions in kMC will replicate this behavior. The shell generated around the kMC droplet is shown as yellow ring around the droplet cross section in Fig. 2(b) and it contains all ions exposed directly to the electric field. The number of ions flagged as shell depends on the instantaneous radius of the primary droplet. Both cations and anions will be part of the shell and become available for emission. Not all ions flagged in the shell will have equal probability of emission. A cation or anion with the lowest Coulomb energy will have the highest probability of emission. The Coulomb energy of the ions located in the shell is calculated as,

$$E_{Coul_i} = C \sum_{\substack{j=1 \\ i \neq j}}^{n} \frac{q_i q_j}{r_{ij}} \tag{3}$$

where, i is the index of ions within the flagged shell, n is the total number of ions in the droplet, q_i and q_j are the charges on the kMC sites i and j, respectively. Only ten ions with the lowest Coulomb energy in the shell are maintained flagged for emission and the remaining ion pairs in the shell are flagged off. The fragmentation step is then performed by randomly selecting one of the ten flagged kMC ions for emissions.

Until this step, all the previous steps performed in the kMC simulations rely on Eqs. 1 and 2 to determine fragmentation criterion. However, theoretical models do not provide the information of secondary species emitted during fragmentation. MD simulations of droplet fragmentation can be used to provide emission species information for the kMC simulations in the form of emission species probability. From our MD simulations, at higher electric field strengths, EMIM-$EtSO_4$ droplets were observed to emit comparatively more dimers and trimer in the positive emission mode than monomers during droplet fragmentation.[29] This information can be transferred to kMC in the form of probabilities. As an example, for EMIM-$EtSO_4$ droplet fragmentation, approximately two dimers will be emitted for every monomer emitted from the droplet. This is implemented in the kMC algorithm using an acceptance-rejection algorithm. To implement the higher rate of dimer-to-monomer emission from an EMIM-$EtSO_4$ droplet, a random number is generated from a uniform distribution between zero and one, and if this random number is less than 0.70, then the dimer emission sequence is executed in the algorithm, else a monomer emission is executed. Over multiple emission iterations, this will result in approximately twice the number of dimers emitted for a given number of monomer emission. The value of 0.70 is the probability of dimer emission compared to monomer emission obtained from either MD or experiments. This ratio depends on the electrochemistry of the ionic liquid, in particular, the Coulomb interactions, H-bond network, and the strength of the applied electric field.

Monomer emissions can be modeled in kMC simply by detaching one of the flagged kMC cells and moving it away from the from the primary droplet structure. Emission of dimers and trimers is more complex. In the positive mode, to model dimer emission from a droplet, one original flagged kMC cell as well as additional cation and anion sites surrounding the original flagged cell will be removed. Similarly, two cation and one anion cells attached to

the original flagged cell will be removed to model trimer emission in the positive emission mode.

The maximum variation in the applied fields will occur near the mouth of the capillary. As stated in our previous work,[27] the normal electric field in the region between the tip of the Taylor cone and the extractor plane will not change significantly and will weaken as the droplet approaches the annulus of the extractor plate. Furthermore, dimers, trimers and droplets with more than nine cation-anion pairs are primarily emitted from the tip of the Taylor cone and will travel along the central axis of the domain, where the radial field is constant and weak. Therefore, the droplet kMC fragmentation simulations are performed considering a constant normal and radial electric field strengths of 3.5 and 0.05 V/nm, respectively. Results from our previous work[27] will be used to create a dataset which will be used as kMC emission probability for monomer, dimer, and trimer secondary emission as a function of applied external electric fields.

The Coulomb fission model also allows one to calculate the break-up time of the secondary emission as an inverse of the primary droplet perturbation growth rate, α_m,

$$t_{break} = \frac{1}{\alpha_m}. \tag{4}$$

The perturbation growth rate is related to the physical and electro-chemical properties of the IL and may be written as,

$$\alpha_m = \left(\frac{4\sigma^6}{27\epsilon^3\gamma^2\rho}\right)^{1/2} \tag{5}$$

where, $\epsilon = 35$ is the dielectric permittivity[30] of EMIM-EtSO_4 and σ, the surface charge density is calculated by,

$$\sigma = \left(\frac{27\epsilon^3\gamma^2\rho I}{4\pi^2 r^4}\right)^{1/8} \tag{6}$$

and, the surface current, I, is calculated using,

$$I = \left(\frac{3\pi^6\epsilon\gamma^2}{2^6\rho}\right)^{1/2}. \tag{7}$$

The evaluated t_{break} is added to a cumulative value, which represents the time progression of the kMC simulation. The t_{break} depends on the radius of the primary droplet and therefore, after every fragmentation event, the droplet radius is re-evaluated to calculate new t_{break}. After this step, all kMC sites are re-flagged ineligible for fragmentation, which is shown as 'Close shell' stage in Fig. 1. We verify if the total number of excess charges in the droplet is lower than the charge criterion determined at the beginning of the simulation, if so the simulation is stopped, else, we execute the motion subroutine.

The motion subroutine ensures that the primary droplet and emitted species are moving in accordance with the applied electric field. The acceleration due to applied electric field on the primary droplet and emitted specie sites is given by,

$$F_i = m_i\vec{a_i} = q_i\vec{E}$$
$$\vec{a_i} = \frac{q_i\vec{E}}{m_i}$$

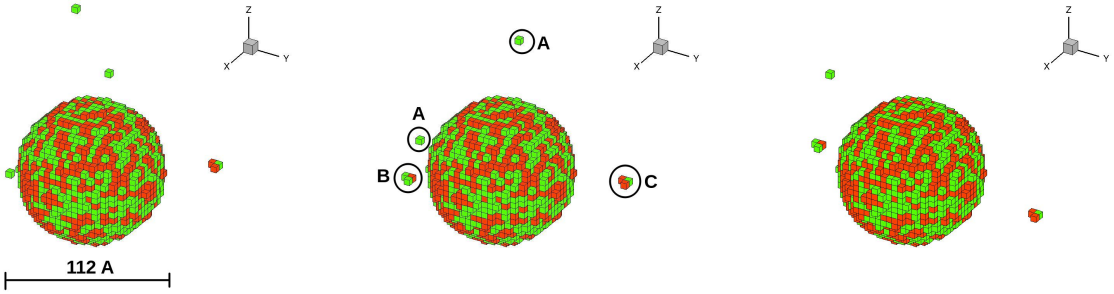

(a) At t = 55 ps (b) At t = 70 ps (c) At t = 97 ps

Figure 3. Trajectory snapshots from droplet fragmentation kMC simulation.

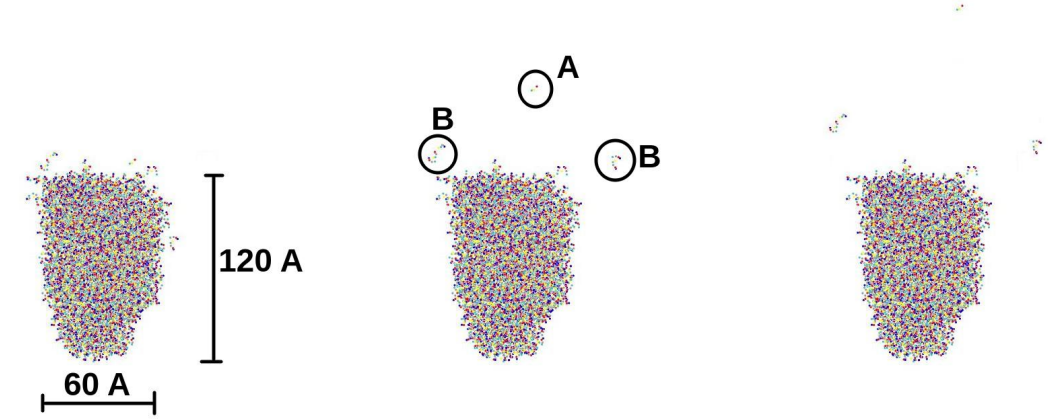

(a) At t = 50 ps (b) At t = 75 ps (c) At t = 100 ps

Figure 4. Trajectory snapshots from droplet fragmentation kMC simulation.

where, $\vec{a_i}$ is the acceleration on the ith ion kMC site due to the external electric field, $\vec{E}$. m_i and q_i is the mass and charge associated with the kMC sites of the primary droplet as well as the emission species. Typically, a cation and anion sites will carry a charge of +1 and -1 e, respectively. However, in kMC, the charge assigned to each site, regardless if it is a cation or anion, will be $q = 1/(n_{cation} + n_{anion})$, where n_{cation} and n_{anion} are the number of cations and anions forming the primary droplet after each iteration. In MD, the ion-pairs are held together by Coulomb interactions and nano-structure induced hydrogen bonding. However, kMC sites are simplified representations of actual ion-pairs, solely using kMC site based Coulomb interactions which cannot counteract the effects of applied electric field. When the acceleration due to the electric field is evaluated for two neighboring kMC sites, representing a cation and an anion pair, it will have opposing effects on the cation and anion due to the polarity of the electric field and the partial charges of +1 and -1e carried by the cations and anions, respectively. This will create an unrealistic instantaneous fragmentation of the primary droplet during the movement phase of the kMC simulation. To avoid this behavior, an equal partial charge is assigned to all sites forming the primary droplet enabling cohesive

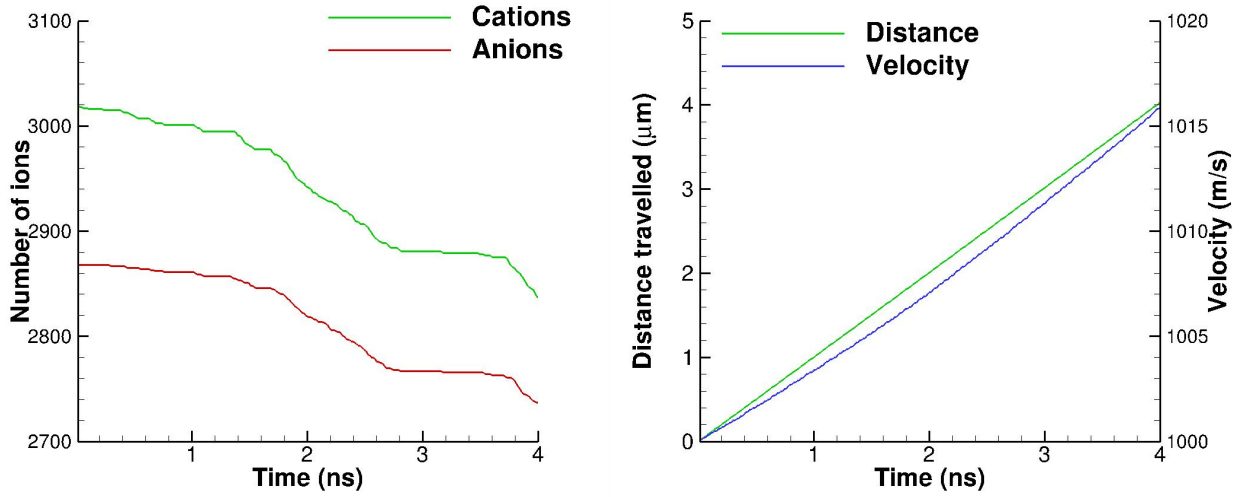

(a) Ion loss from primary droplet

(b) Distance and velocity of primary droplet

Figure 5. Ion loss from and the velocity of the primary droplet in a constant electric field.

motion of the entire droplet geometry to prevent from splitting into counter-moving cations and anions due to the polarity of the applied electric field. Using the same strategy, each site of the trimers and dimers emitted during fragmentation are also assigned charge values of 1/5 and 1/3 e, for cation species, and -1/5 and -1/3 e for anion species, respectively. Only the cation and anion monomers are assigned a charge of 1 and -1 e, respectively. The mass assigned to each site is also similarly averaged depending on the number of cations and anions forming the primary droplet or the emission species. The droplet and the kMC sites are then moved using the Leap-frog integration,[31]

$$\vec{v}_{t+1/2} = \vec{v}_t + \vec{a}_t \frac{t_{break}}{2}$$
$$\vec{x}_{t+1} = \vec{x}_t + \vec{v}_{t+1/2} t_{break}$$
$$\vec{v}_{t+1/2} = \vec{v}_{t+1/2} + \vec{a}_{t+1} \frac{t_{break}}{2}$$

The trajectory snapshots of the fragmentation process of primary droplets obtained from the kMC simulation are shown in Fig. 3. For comparison, snapshots from the MD simulation of droplet fragmentation simulation are shown in Fig. 4. The emitted positive monomer, positive dimer, and negative dimer species are labeled as A, B, and C, respectively.

At the completion of the motion subroutine, the displacement of the primary droplet sites is subtracted from all displaced ion sites. This ensures that the slow-moving primary droplet retains the central location in the kMC grid, allowing the simulation to proceed until the charge criterion check is met. The charge loss from the 150 cation bias EMIM-$EtSO_4$ droplet is shown in Fig. 5(a). Initially, the primary droplet contains 150 more cations compared to the anions, which reduces to 98 extra cations compared to the anions at the end of the fragmentation process. The distance traveled and the velocity of the primary droplet are shown in Fig. 5(b), where, using KMC, we were able to model the droplet motion while performing fragmentation on the micrometer length scale.

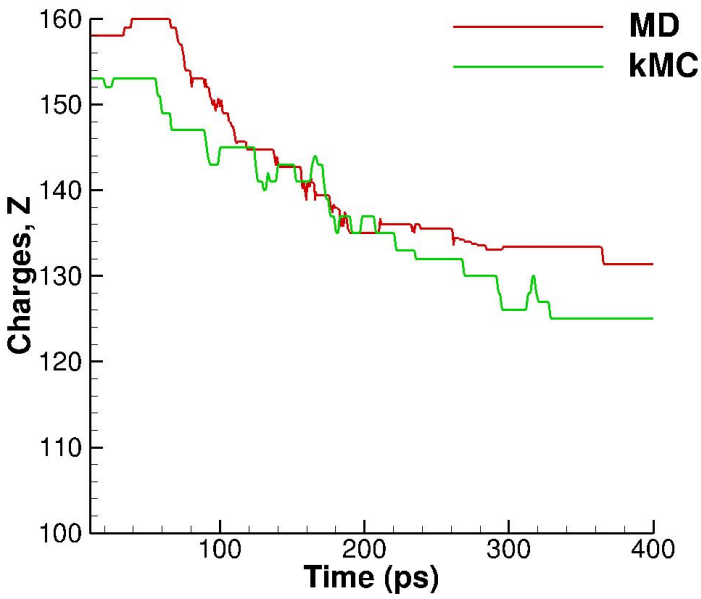

Figure 6. Comparison of charge loss from a EMIM-BF_4 droplet with approximately 150 cation bias.

III. Results and discussion

A. Comparison of charge loss with MD

A kMC simulation was performed for EMIM-BF_4 droplet with 155 extra cations to compare the charge loss behavior with that from MD for a similar droplet. The time between two fragmentation events, i.e., t_{break}, predicted by Eq. 4 was a factor of four higher than that observed from MD. We attribute this discrepancy to the difference in the shape of the droplet. For the MD simulation, the IL droplet had a teardrop shape, with IL material forming apex at the two poles. In contrast, we assumed a perfectly spherical droplet. The electric field will be considerably more effective at removing ions from a teardrop shaped droplet. To account for this, the t_{break} obtained from Eq. 4 was always reduced by a factor of four during the kMC simulation. The comparison of MD and kMC droplet charge loss from the simulations is shown in Fig. 6. As seen in Fig. 6, the kMC simulation was able to reproduce the loss of 28 cation species in 400 ps, which is in a good agreement with the charge loss and time predicted by MD.

B. Effect of surface tension on droplet fragmentation behavior

As discussed previously, fragmentation will depend on the electrochemical properties of the ILs and the emission species probabilities predicted by MD simulations. To understand the differences generated in the emission characteristics due to these parameters, we performed fragmentation simulations of EMIM-$EtSO_4$ and EMIM-BF_4. Both ILs are aprotic and have similar cation-anion RDFs as well as mass densities. There is a noticeable difference between the surface tension of the two ILs: 57 mN/m for EMIM-$EtSO_4$, as determined by

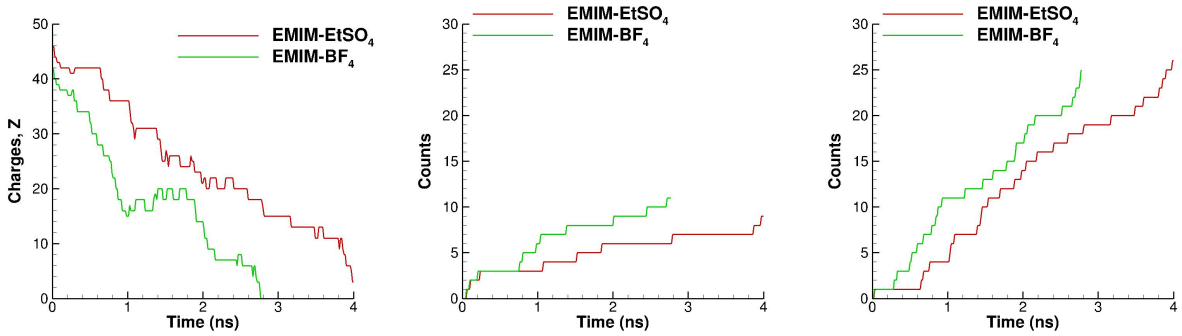

(a) Charge loss comparison (b) Cation monomer emission comparison (c) Cation dimer emission comparison

Figure 7. Comparison of charge, monomer, and dimer loss from EMIM-EtSO$_4$ versus EMIM-BF$_4$ kMC simulations.

Wainwright and Rovey, whereas, that of EMIM-BF$_4$ at room temperature is 47 mN/m.[32] Also, the dielectric permittivity of both ILs is significantly different, 35 for EMIM-EtSO$_4$[30] versus 15 for EMIM-BF$_4$.[33] The emission species probabilities for the two ILs are similar, 0.30 for EMIM-EtSO$_4$[29] versus 0.34 for EMIM-BF$_4$,[27] as determined from our previous MD simulations.

Comparison of the total charges lost during the simulation is shown in Fig. 7(a). It can be observed that the charge loss rate is higher from the BF$_4$ based IL droplet. This is due to a combination of significantly lower surface tension and dielectric permittivity of EMIM-BF$_4$, both of which, allow easy movement of ions by weakening the droplet surface. This will result in smaller t_{break} for EMIM-BF$_4$ fragmentation leading to faster charge loss. As expected, the monomer and dimer emission counts are the same for both ILs, as shown in Figs. 7(b) and 7(c), respectively, because both ILs have similar emission probabilities. Although, the loss rate of EMIM-BF$_4$ is higher due to the aforementioned differences in the surface tension and dielectric permittivity.

To better understand the individual effects of surface tension and dielectric permittivity, kMC simulations were performed by considering a fixed dielectric permittivity and varying the surface tension of the IL droplet. For this analysis, a fragmentation simulation was performed for an EMIM-BF$_4$ droplet with a radius of 56 Å and a cation bias of 150. A comparison of a polynomial fit (order 3) of the charge loss as a function of simulation time is shown in Fig. 8(a). When the surface tension was increased from its baseline value of 47 mN/m to that of EMIM-ETSO$_4$, 57 mN/, the charge loss was comparatively faster. When the surface tension was arbitrarily lowered to 37 mN/m, the droplet fragmentation was gradual. Surface tension, γ is directly proportion to the Rayleigh instability, Eq. 1 and approximately square root proportionality to the t_{break}, as shown in Eqs. 4 and 5. It must also be notes that the instantaneous radius of the droplet is also changing as it loses ions, as shown in Fig. 8(b) The combined effect is to have faster ion loss during fragmentation for the higher surface tension. In contrast, when the surface tension was kept constant and the dielectric permittivity was varied, there was no significant change in the charge loss behavior.

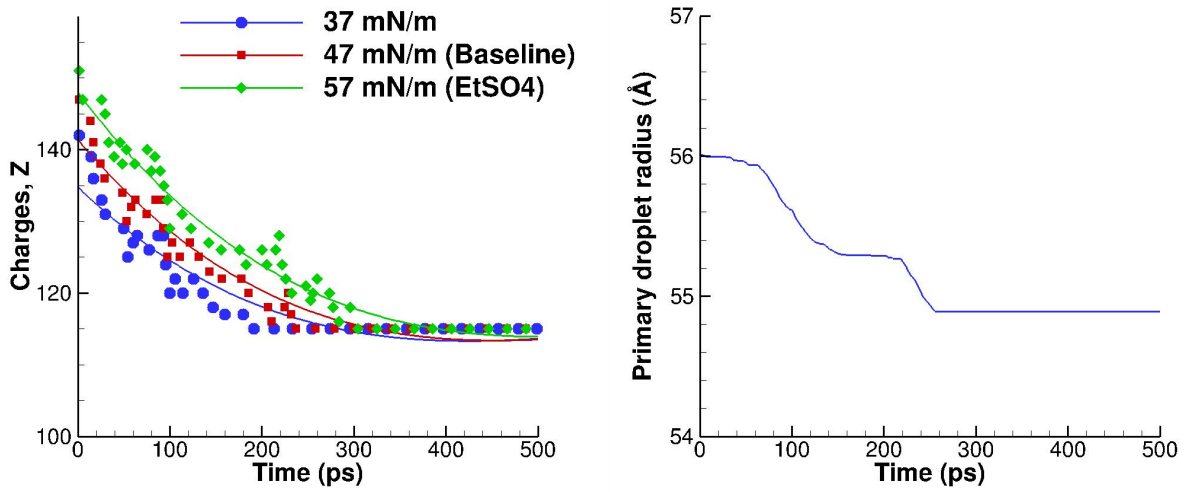

(a) Change due to surface tension

(b) Primary droplet radius

Figure 8. Effect of surface on kMC predicted charge loss and instantaneous primary droplet radius.

C. Effect of cation bias and droplet radius on charge loss rate

As defined previously, the charge bias is the number of additional cations in the droplet. To understand the role of charge bias on charge loss, we performed kMC simulations of EMIM-BF_4 by keeping all the electrochemical properties the same but the charge bias of the droplet was changed. As shown in Fig. 9(a), changing the droplet bias does not affect the slope of the charge loss curve. However, the curves shift proportional to the bias and determine the y-intercept of the charge loss as a function of simulation time. In comparison, the initial droplet radius has a significant impact on the charge loss behavior. When the radius of the IL droplet is reduced, the charge loss from the droplet is slower and vice-versa, as shown in Fig. 9(b). Unlike the effects of varying either surface tension or droplet bias, the effects of changing the droplet radius cannot be easily generalized. When the droplet radius was changed, the charge loss behavior, its starting y-intercept and its end charge, all are affected. The kMC simulations predicted that a droplet with an initially larger radius, for same cation bias, will have more ion-pairs, leading to more cations over the Rayleigh limit criterion. A larger radius will also lower the t_{break} between two successive fragmentation events. Both these effects combine to create a complex charge loss behavior when analyzed by changing the droplet radius.

IV. Conclusions and future work

In this work, we propose a kMC algorithm to simulate IL droplet fragmentation, allowing possible scale bridging of MD fragmentation results from nanometer and nanosecond length scales to micrometer and microseconds. The kMC algorithm relies on Rayleigh instability theory and ion emission model to determine fragmentation criterion. We used the MD derived monomer, dimer, and trimer emission probabilities to model emission during kMC fragmentation events. Time between every successive emission event was determined from

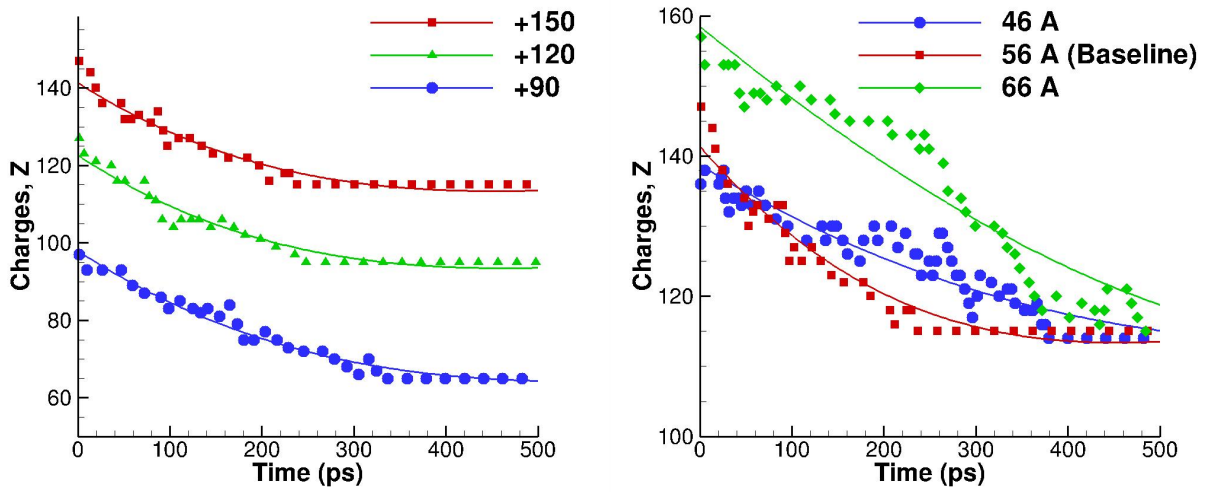

(a) Change due to charge bias

(b) Change due to droplet radius

Figure 9. Effect of droplet bias and radius on kMC predicted charge loss.

the CRM and IEM models. Using this kMC approach, we obtained charge loss behavior of a prototypical EMIM-BF_4 droplet, which was in good agreement with the charge loss from an MD simulation. The fragmentation results from kMC will be used by coupling them with the in-house CHAOS PIC code. This future work can be broken down into three distinct steps. These steps represent project milestones with increasing difficulty.

A. Electrospray plume expansion in free space using CHAOS

Our in-house PIC code CHAOS has been used for ion thruster plume propagation. It is a massively parallel multi-CPU-GPU code with adaptive mesh capability. One of the current unknowns with regards to electrospray thrusters is the detailed computational analysis of plume propagation beyond the extractor plane in space as well as in experimental facilities. Having this knowledge will allow us to better predict electrospray impingement on satellite surfaces and their effects. In the region away from the extractor plate, ions emitted from the electrospray will experience only a weak ambient electric field. Therefore, these weak electric fields will not affect the propagation of ion species and also larger emission products, such as, dimers and trimers will likely not fragment into smaller species. The plume expansion will occur primarily due to the exhaust velocities of the emission species.

To simulate the electrospray beam, we will use the emission results obtained from our MD simulations. We will calculate the mass flow rate, exhaust velocities, and emission angles of these ion species, and use those as an input for the PIC code. We will use CHAOS in the multi-species configuration such that monomers, dimers, and trimers will be treated as individual species. Each computational particle of a specie represents either one monomer, dimer, or a trimer. It must be noted that MD simulations are performed at lower mass flow rates (¡ 10^{-11} kg/s), thereby, generating only monomers, dimers, and trimers as emission species. At higher mass flow rates, electrosprays will generate large droplets. Based on the kMC algorithm, we can determine the final fragmentation products of these large droplets

thus obtaining an overall mass flow rate of emission species beyond the extractor plane.

Initially, we will not model collisions between the emission species. For the first simulation cases, only the collision less propagation of multi species jet will be modeled. This step will provide us with a baseline regarding the plume propagation extent, allowing us to determine the domain size required for such a simulation. This simulation should be treated as an initial step in determining Neumann and Dirichlet boundary conditions necessary to generate weak electric field. Increasing the complexity, for the next simulation, we will perform electrospray beam propagation with inter-species collision. However, we will require collision cross sections between the three species emitted from the electrospray. This will be done by performing trajectory simulations of inter-species collision using MD. Collision cross sections obtained from MD will be used as an input to perform coupled PIC DSMC simulations of plume propagation.

B. Derive kMC algorithm to reproduce Taylor cone formation and emission

As mentioned previously, we have performed MD electrospray simulations at low mass flow rates (¡ 10^{-11} kg/s) due to computational limitations. Electrospray simulations at higher mass low rates will require a larger domain because the ejected ion species will start filling out a smaller domain and lead to unrealistic interactions between Taylor cone and emitted ion species. As processors are mapped to the domain, increasing the computational domain will lead to a large number of processors mapping regions with no ions present leading to a very inefficient simulation. An alternative approach would be to use the observations from MD as well as theoretical models to derive an kMC algorithm capable of recreating the Taylor cone at micrometer length scale as opposed to nanometers currently feasible with MD.

In order to replicate Taylor cone formation using kMC, we will have to improve our droplet fragmentation kMC algorithm in two key areas. For the droplet simulation, we use the same sized grid cells for both, cation and anion. Furthermore, the cation and anions locations are assigned randomly and with bias. This is a valid strategy for droplet simulation but when modeling electrospray from bulk, kMC cation and anion grid cells will have to be arranged based on the coordination number, unique to each IL. Before moving to the second part of this step, we will perform kMC simulations of IL bulk in the absence of external electric field to compare the nanostructure and electrochemical properties of kMC bulk with those obtained from MD. The second improvement will be to impose Taylor cone shape on the IL bulk modeled by kMC. The grid cells should be adequately fine to accurately resolve the Taylor cone shape. The Taylor cone geometry will be modeled using the theoretical expressions from the work by Krpoun and Shea.[34]

C. Multi-capillary electrospray kMC simulation

Typical electrospray devices operate as an array of emitters as opposed to a solo emitter. There will be interaction between the emission products from one capillary and another due to beam spreading. For this part of the project, we will integrate the changes made for the two steps described above. Coupled PIC-DSMC simulations will be performed using kMC to generate the plume emission products. The emission species will be allowed to collide and generate backflow, which is an area of interest for this work. All three steps combined will

allow us to create a complete computational model of electrospray thruster device, results from which will be compared with the experimental measurements.

Acknowledgments

Funding for this work was provided by the NASA ESI through Dr. Thomas Liu under Grant No. 80NSSC19K0215. We are thankful to the XSEDE TACC for allowing computational resources on their STAMPEDE2 cluster.

References

[1]Taylor, G. I., "Disintegration of Water Droplets in an Electric Field," *Proceedings of Royal Society A*, Vol. 280, No. 1328, 1964, pp. 383–397.

[2]Deng, W., Waits, C. M., and Gomez, A., "Digital electrospray for controlled deposition," *Review of Scientific Instruments*, Vol. 81, No. 3, March 2010, pp. 035114.

[3]Jaworek, A., "Electrospray droplet sources for thin film deposition," *Journal of Materials Science*, Vol. 42, No. 1, January 2007, pp. 266–297.

[4]Swanson, L., "Liquid metal ion sources: Mechanism and applications," *Nuclear Instruments and Methods in Physics Research*, Vol. 218, No. 1, December 1983, pp. 347–353.

[5]Clampitt, R., "Advances in molten metal field ion sources," *Nuclear Instruments and Methods in Physics Research*, Vol. 189, No. 1, October 1981, pp. 111–116.

[6]Wu, Y., Kennedy, S. J., and Clark, R. L., "Polymeric particle formation through electrospraying at low atmospheric pressure," *Journal of Biomedical Materials Research Part B: Applied Biomaterials*, Vol. 90B, No. 1, 2009, pp. 381–387.

[7]Zhu, W., Castro, N. J., Cheng, X., Keidar, M., and Zhang, L. G., "Cold Atmospheric Plasma Modified Electrospun Scaffolds with Embedded Microspheres for Improved Cartilage Regeneration," *PLoS ONE*, Vol. 10, No. 7, 07 2015, pp. e0134729.

[8]Wu, B. and Becker, J. S., "Imaging of elements and molecules in biological tissues and cells in the low-micrometer and nanometer range," *International Journal of Mass Spectrometry*, Vol. 307, No. 1, October 2011, pp. 112–122.

[9]Donius, B. and Rovey, J. L., "Ionic Liquid Dual-Mode Spacecraft Propulsion Assessment," *Journal of Spacecraft and Rockets*, Vol. 48, No. 1, 2011, pp. 110–123.

[10]Prince, B. D., Tiruppathi, P., Bemish, R. J., Chiu, Y.-H., and Maginn, E. J., "Molecular Dynamics Simulations of 1-Ethyl-3-methylimidazolium Bis[(trifluoromethyl)sulfonyl]imide Clusters and Nanodrops," *The Journal of Physical Chemistry A*, Vol. 119, No. 2, 2015, pp. 352–368.

[11]P., A. M. and Tildesley, D. J., *Computer Simulations of Liquids*, Oxford Science Publications, 2009.

[12]Romero-Sanz, I., Bocanegra, R., Fernandez de la Mora, J., and Gamero-Castano, M., "Source of heavy molecular ions based on Taylor cones of ionic liquids operating in the pure ion evaporation regime," *Journal of Applied Physics*, Vol. 94, No. 5, June 2003, pp. 3599–3605.

[13]Mehta, N. A. and Levin, D. A., "Effects of Long-range Coulomb interaction models on the Electrospray Molecular Dynamics Simulations," *Physical Review E*, under review.

[14]Gomez, A. and Tang, K., "Charge and fission of droplets in electrostatic sprays," *Physics of Fluids*, Vol. 6, No. 1, 1994, pp. 404–414.

[15]Duft, D., Achtzehn, T., Muller, R., Huber, B. A., and Leisner, T., "Coulomb fission: Rayleigh jets from levitated microdroplets," *Nature*, Vol. 421, No. 128, January 2003, pp. 1.

[16]Li, D., Marquez, M., and Xia, Y., "Capturing electrified nanodroplets under Rayleigh instability by coupling electrospray with a sol–gel reaction," *Chemical Physics Letters*, Vol. 445, No. 4, 2007, pp. 271 – 275.

[17]Ichiki, K. and Consta, S., "Disintegration Mechanisms of Charged Aqueous Nanodroplets Studied by

Simulations and Analytical Models," *The Journal of Physical Chemistry B*, Vol. 110, No. 39, September 2006, pp. 19168–19175.

[18]Marginean, I., Znamenskiy, V., and Vertes, A., "Charge Reduction in Electrosprays Slender Nanojets as Intermediates," *The Journal of Physical Chemistry B*, Vol. 110, No. 12, March 2006, pp. 6397–6404.

[19]Giglio, E., Gervais, B., Rangama, J., Manil, B., Huber, B. A., Duft, D., Müller, R., Leisner, T., and Guet, C., "Shape deformations of surface-charged microdroplets," *Physical Review E*, Vol. 77, March 2008, pp. 036319.

[20]Constantopoulos, T. L., Jackson, G. S., and Enke, C. G., "Challenges in achieving a fundamental model for ESI," *Analytica Chimica Acta*, Vol. 406, No. 1, February 2000, pp. 37 – 52.

[21]Dole, M., Mack, L. L., Hines, R. L., Mobley, R. C., Ferguson, L. D., and Alice, M. B., "Molecular Beams of Macroions," *The Journal of Chemical Physics*, Vol. 49, No. 5, 1968, pp. 2240–2249.

[22]Iribarne, J. V. and Thomson, B. A., "On the evaporation of small ions from charged droplets," *The Journal of Chemical Physics*, Vol. 64, No. 6, 1976, pp. 2287–2294.

[23]Rayleigh, L., "XX. On the equilibrium of liquid conducting masses charged with electricity," *Philosophical Magazine*, Vol. 14, No. 87, 1882, pp. 184–186.

[24]Bortz, A., Kalos, M., and Lebowitz, J., "A new algorithm for Monte Carlo simulation of Ising spin systems," *Journal of Computational Physics*, Vol. 17, No. 1, 1975, pp. 10 – 18.

[25]Schaefer, C. and Jansen, A. P. J., "Coupling of kinetic Monte Carlo simulations of surface reactions to transport in a fluid for heterogeneous catalytic reactor modeling," *The Journal of Chemical Physics*, Vol. 138, No. 5, 2013, pp. 054102.

[26]Mehta, N. A., Rayabharam, R., and Levin, D. A., "Simulations of surface evolution due to particulate-surface interaction," *AIAA Scitech 2019*, 2019, pp. 1–38.

[27]A., M. N. and Levin, D. A., "Colloid thruster droplet evolution analysis using molecular dynamics," *35th International Electric Propulsion Conference Atlanta-Georgia, USA*, Vol. IEPC-2017-66, 2017, pp. 1–21.

[28]Hogan, C. J., Carroll, J. A., Rohrs, H. W., Biswas, P., and Gross, M. L., "Combined Charged Residue-Field Emission Model of Macromolecular Electrospray Ionization," *Analytical Chemistry*, Vol. 81, No. 1, 2009, pp. 369–377.

[29]A., M. N. and Levin, D. A., "Study Of Ionic Liquid Mixture Droplet Evolution In An External Electric Field Using Molecular Dynamics," *31st International Symposium on Rarefied Gas Dynamics, Scotland*, 2018, pp. 1–7.

[30]Huang, M.-M., Jiang, Y., Sasisanker, P., Driver, G. W., and Weingärtner, H., "Static Relative Dielectric Permittivities of Ionic Liquids at 25 °C," *Journal of Chemical & Engineering Data*, Vol. 56, No. 4, 2011, pp. 1494–1499.

[31]Langdon, A. B. and Birdsall, C. K., *Plasma Physics via Computer Simulation*, CRC Press, 1985.

[32]Liu, W., Zhao, T., Zhang, Y., Wang, H., and Yu, M., "The Physical Properties of Aqueous Solutions of the Ionic Liquid [BMIM][BF4]," *Journal of Solution Chemistry*, Vol. 35, No. 10, Oct 2006, pp. 1337–1346.

[33]Singh, T. and Kumar, A., "Static Dielectric Constant of Room Temperature Ionic Liquids: Internal Pressure and Cohesive Energy Density Approach," *The Journal of Physical Chemistry B*, Vol. 112, No. 41, 2008, pp. 12968–12972.

[34]Krpoun, R. and Shea, H. R., "A method to determine the onset voltage of single and arrays of electrospray emitters," *Journal of Applied Physics*, Vol. 104, No. 6, 2008, pp. 064511.